Electronic properties of bulk and thin film $SrRuO_3$: Search for the metal-insulator transition

James M. Rondinelli,[1] Nuala M. Caffrey,[2] Stefano Sanvito,[2] and Nicola A. Spaldin[1,*]
[1]*Materials Department, University of California, Santa Barbara, California 93106-5050, USA*
[2]*School of Physics and CRANN, Trinity College, Dublin 2, Ireland*
(Received 7 June 2008; revised manuscript received 11 September 2008; published 7 October 2008)

We calculate the properties of the 4*d* ferromagnet $SrRuO_3$ in bulk and thin film form with the aim of understanding the experimentally observed metal-to-insulator transition at reduced thickness. Although the spatial extent of the 4*d* orbitals is quite large, many experimental results have suggested that electron-electron correlations play an important role in determining this material's electronic structure. In order to investigate the importance of correlation, we use two approaches which go beyond the conventional local-density approximation to density-functional theory (DFT): the local spin-density approximation+Hubbard *U* (LSDA+*U*) and the pseudopotential self-interaction correction (pseudo-SIC) methods. We find that the details of the electronic structure predicted with the LSDA do not agree with the experimental spectroscopic data for bulk and thin film $SrRuO_3$. Improvement is found by including electron-electron correlations, and we suggest that bulk orthorhombic $SrRuO_3$ is a moderately correlated ferromagnet whose electronic structure is best described by a 0.6 eV on-site Hubbard term, or equivalently with corrections for the self-interaction error. We also perform *ab initio* transport calculations that confirm that $SrRuO_3$ has a negative spin polarization at the Fermi level, due to the position of the minority Ru 4*d* band center. Even with static correlations included in our calculations we are unable to reproduce the experimentally observed metal-insulator transition, suggesting that the electronic behavior of $SrRuO_3$ ultrathin films might be dominated by extrinsic factors, such as surface disorder and defects, or due to dynamic spin correlations which are not included in our theoretical methods.

DOI: 10.1103/PhysRevB.78.155107 PACS number(s): 71.20.−b, 79.60.Dp, 32.10.Dk

I. INTRODUCTION

Conductive oxides are essential components in composite oxide heterostructures where they are often used as electrode materials in thin film applications.[1–3] In the perovskite crystal family (ABO_3 stoichiometry), the itinerant ferromagnetic $SrRuO_3$ (SRO) is a popular choice since it is one of the more conductive metallic oxides with good thermal properties.[4] In thin films, SRO is intensely investigated as a possible route to the realization of novel field-effect devices.[5,6] In addition, it is of particular interest to the spintronic[7,8] and multiferroic[9,10] communities, which have been recently energized by the possible device applications available from engineering interface phenomena.[11–17] However, one limitation in the design of thin film oxide devices is the observation of increased resistivity in metal oxides as the film thickness decreases. Such behavior is clearly present in ultrathin films of $SrRuO_3$, where a metal-to-insulator (MI) transition[18] occurs at four monolayers. This substantial change in the electrical conductivity presents a serious challenge for device miniaturization. In this work we explore the underlying physics of the thin film MI transition, which to date remains to be understood.

The 3*d* transition-metal oxides (TMOs) are known to possess strong electron-electron correlation effects that can drive a system that should be metallic within a simple band picture into an insulating state. Due to the large spatial extent of the 4*d* orbitals in the ruthenates, correlation effects are anticipated to be less important as stronger hybridization provides more effective screening and a reduced Hubbard *U* (Coulomb repulsion energy). Many experimental studies have already addressed the degree of electron-electron correlation in $SrRuO_3$ including x-ray and ultraviolet photoemission spectroscopy,[18–21] specific-heat measurements,[22] infrared and optical conductivity measurements,[23] and transport experiments.[24] For example, Kim and co-workers[19] use x-ray photoemission spectroscopy (XPS) to identify how such correlations change within the ruthenate family, and Toyota *et al.*[18] use photoemission spectroscopy (PES) to detail the metal-insulator transition in $SrRuO_3$ as a function of film thickness concomitant with the onset of magnetism. In all of these studies, the general consensus is that electron correlation effects *do* play a role in determining the electronic structure of this itinerant ferromagnet, but to what degree remains unclear. Furthermore, some theoretical investigations have begun examining covalency,[25] correlation[26] and orbital ordering[27] effects in bulk $SrRuO_3$. The magnetic properties of SRO under epitaxial strain have also been investigated with first-principles techniques.[28]

In this work, first-principles density-functional theory (DFT) calculations are performed, first to identify the degree of correlation in bulk SRO, and second to investigate the driving force for the metal-insulator transition in ultrathin films. We use two approaches to introduce correlation effects into the conventional band theory (local spin density) approach for treating the Ru 4*d* orbitals and their hybridization with O 2*p* orbitals: the local spin density+Hubbard *U* (LSDA+*U*), and the pseudopotential self-interaction corrected (pseudo-SIC) local spin-density methods. In addition we investigate two structural variants—the ideal cubic perovskite structure and the experimentally observed orthorhombic structure, which includes tiltings and rotations of the RuO_6 octahedra. By comparing the results that we obtained for both methods and both structure types, we are able to comment on the nature of the metal-insulator transition in ultrathin films.

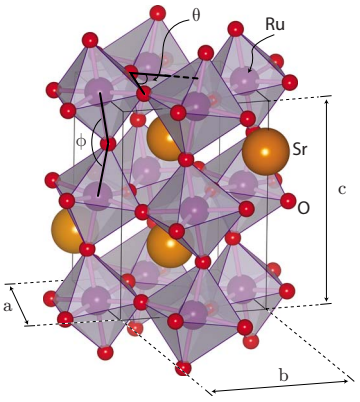

FIG. 1. (Color online) The orthorhombic (*Pbnm*) crystal structure of $SrRuO_3$. The unit cell contains four formula units (f.u.) of the ideal cubic perovskite ($Pm\bar{3}m$). The structure is stabilized by shortening the Sr-O distance followed by a cooperative distortion of the RuO_6 octahedra to reduce the coordination volume of the Sr ions; this results in a smaller Ru-O-Ru bond angle, which in turn decreases the Ru 4*d* bandwidth and metallicity. The deviation in the structure from the high symmetry cubic state can be quantified using the tilting angle $(180°-\phi)/2$ and the rotation angle $(90°-\theta)/2$ of the oxygen octahedra.

II. CRYSTAL STRUCTURE AND MAGNETISM

The perovskite class of materials is described by a network of corner-sharing BO_6 octahedra, in which the *A*-site cation is located at the center of a cube defined by eight BO_6 units. The ideal perovskite is cubic (space group $Pm\bar{3}m$), however several modifications exist owing to the range of cation sizes that can be accommodated in the structure. Deviations from the ideal cubic structure are defined by the Goldschmidt tolerance factor

$$t' = \frac{R_A + R_O}{\sqrt{2}(R_B + R_O)},$$

where R_i is the radius of atom *i*, and can be attributed to the requirement to optimize the anion coordination about the *A*-site cation.[29] Using the Shannon-Prewitt radii for this compound, a predicted tolerance factor of $t'=0.908$ is found, which is far from the ideal case $t'=1$, suggesting that distortions should occur.

Indeed, SRO undergoes a series of structural transformations with temperature, from high symmetry cubic ($Pm\bar{3}m$, stable above 950 K) to tetragonal ($I4/mcm$, stable between 820 and 950 K) to distorted orthorhombic structure (*Pbnm*) at low temperatures. The orthorhombic distortion from the ideal cubic can be described by the tilting of the RuO_6 octahedra in alternate directions away from the *c* axis, and the rotation of the octahedra around the *b* axis; in both cases adjacent octahedra distort in the opposite sense (Fig. 1).

The degree of tilting and rotation (as defined in Fig. 1) of the octahedra are useful in describing the distortions in the oxygen network from the perfect cubic case. A rotation angle of 7.56° and a tilting angle of 10.47° (corresponding to a Ru-O-Ru angle of 159°) are found for *Pbnm* $SrRuO_3$. The structural changes reduce the hybridization between the Ru 4*d* states and O 2*p* states and lead to a narrowing of the bandwidths (see Sec. IV) compared with the ideal cubic case. Consequently the degree of correlation, described by U/W where *W* is the valence bandwidth, is expected to be enhanced.

Below approximately 160 K, $SrRuO_3$ exhibits strong ferromagnetic behavior, and has a measured Rhodes-Wohlfarth ratio[30] ($\mu_{\text{eff}}/\mu_{\text{sat}}$) of 1.3 suggesting that its magnetism can be well described by a localized *d*-electron model similar to the elemental ferromagnetic metals. Within this model and under an octahedral crystal field, the 4*d* manifold splits into a threefold degenerate t_{2g} subband that is lower in energy than the twofold degenerate e_g band. Neglecting covalency, we would expect a spin-only magnetic moment of 2 μ_B, corresponding to a low-spin state for the Ru^{4+} ions (d^4:$t_{2g\uparrow}^3, t_{2g\downarrow}^1$). Experimentally, however, the moment in the bulk orthorhombic material is measured to be closer to 1.1 μ_B/f.u., although values ranging from 0.9 μ_B/f.u. and 1.6 μ_B/f.u. have also been reported.[31] (The spread in values is attributed to the large magnetocrystalline anisotropy of the material, and the difficulty in making large single-domain samples.) First-principles calculations also report a magnetic moment ranging from 0.9 μ_B/f.u. to 2.0 μ_B/f.u. depending on the details of the exchange and correlation functional and the treatment of the core and valence electrons.[22–34] The reduced calculated magnetic moment in the solid compared to that in the free ion limit is due in part to the large spatial extent of the Ru 4*d* orbitals, which results in a significant overlap (hybridization) with the oxygen 2*p*. Furthermore, due to the metallic character of SRO, an overlap of the majority and minority Ru 4*d* bands occurs at the Fermi level; as a result partial occupation of the minority band also leads to a reduced magnetic moment.

In this work, we examine the local spin-density approximation (LSDA) and "beyond-LSDA" electronic and magnetic properties of both the *Pbnm* and $Pm\bar{3}m$ crystal variants. Metallicity and magnetism are both related to the *d* bandwidth, which in turn depends on both correlations and structural properties such as tiltings and rotations of the oxygen octahedra. Our goal, therefore, is to identify the relative contributions of electron-electron correlation effects and structural distortions in driving the metal-insulator transition in $SrRuO_3$ thin films.

III. THEORETICAL METHODS

A. LSDA

Our initial electronic band-structure calculations were performed within the LSDA (Ref. 35) using both the SIESTA[36–38] and VASP[39,40] DFT packages. In each method we used the Perdew-Zunger[41] parametrization of the Ceperley-Alder data[42] for the exchange and correlation (XC) functional.

The core and valence electrons were treated with the projector augmented wave (PAW) method[43] for all calculations performed with VASP.[44] Furthermore a plane-wave energy cutoff of 500 eV was used and found to produce excellent convergence. The three-dimensional Brillouin zone was

TABLE I. Results obtained for cubic $SrRuO_3$ within the LSDA from the two codes used in this work. The equilibrium lattice constant relative to the experimental value (a_0=3.9735 Å) determined from high-temperature neutron-diffraction data (Ref. 51), the bulk modulus B, the pressure derivative B', and the magnetic moment per formula unit are given for each code. Very good agreement is found between the two codes. The notations for the codes are as follows: SIESTA: Spanish Initiative for Electronic Simulations with Thousands of Atoms local orbital code and VASP: vienna *ab initio* simulation package plane-wave code.

	VASP	SIESTA
a/a_o	0.98	0.98
B (GPA)	200	219
B'	4.6	4.4
Moment (μ_b/f.u.)	1.09	1.26

sampled with a $12\times12\times12$ k-point Monkhorst-Pack mesh[45] for the cubic bulk (five-atom unit cell) and thin film structures and a $12\times12\times10$ k-point sampling mesh for the bulk orthorhombic structure (20-atom unit cell). For the orthorhombic films we used a $12\times12\times3$ k-point sampling. In all cases the tetrahedron method with Blöchl corrections[46] was used for the Brillouin-zone integrations.

In the localized basis code SIESTA, the core and valence electrons were treated with norm-conserving fully separable[47] Troullier-Martin[48] pseudopotentials.[49] The localized atomic orbitals for each atom used a single-ζ basis set for the semicore states and a double-ζ for the valence states. Total energies were computed on a uniform real space grid with a cutoff of 800 Ry in order to reach comparable accuracy to the plane-wave code.[50] The Brillouin zone of the cubic structure was sampled with a $26\times26\times26$ k-point Monkhorst-Pack mesh, while the *Pbnm* structure was sampled with a $15\times15\times12$ k-point mesh. Integrations were performed with a Gaussian broadening of 0.10 eV in all calculations.

The equilibrium lattice parameter for the cubic structure was found by fitting the total energy as a function of volume to the Murnaghan equation of state. Excellent agreement was found between the two codes (Table I), with a slight underestimate of the experimental lattice constant typical for the LSDA. The cell parameters and atomic positions of the orthorhombic structure (Table II) were optimized by starting from the positions reported in Ref. 28 and the ionic coordinates were relaxed until the Hellmann-Feynman forces on the atoms were less than 4 meV $Å^{-1}$. Investigations of the electronic structure of cubic $SrRuO_3$ have been described by several different groups[22,28,32] within the LSDA; here we briefly summarize their conclusions and remark that our results are consistent with the earlier calculations. A complete comparison of the electronic structure of cubic $SrRuO_3$ calculated with both VASP and SIESTA is made in Sec. IV. In all cases, a metallic ferromagnetic ground state is found to be stable, with strong Ru 4d character at the Fermi level. Substantial hybridization occurs between the O 2p states and the Ru 4d states and no energy gaps are observed in the densities of states (DOSs). The calculated magnetic moment is also always reduced from the fully ionic limit of 2 μ_B.

TABLE II. Calculated structural parameters for $SrRuO_3$ with the *Pbnm* symmetry using VASP. Our calculated orthorhombic lattice constants are a=5.4924, b=5.4887, and c=7.7561 Å.

Atom	Site	x	y	z
Sr	4c	–0.0050	0.03039	0.25
Ru	4a	0.5	0.0	0.0
O(1)	4c	0.0650	0.4942	0.25
O(2)	8d	0.7158	0.2834	0.0340

B. LSDA+U

The first "beyond-LSDA" method that we use to treat the XC within DFT is the local spin-density approximation with Hubbard U (LSDA+U).[52] Here we use the spherically averaged form of the rotationally invariant LSDA+U introduced by Dudarev *et al.*,[53] in which only one effective Hubbard parameter, $U_{\text{eff}}=U-J$, is used, where U and J are the spherically averaged Hubbard repulsion and intra-atomic exchange for electrons with the angular momentum of interest; in this case Ru 4d states. We treat the double-counting term within the fully localized limit and note that this should more correctly describe the insulating side of the metal-insulator transition that we study here; an improved description of the metallic side might be achieved using the recently introduced interpolation between the around-mean-field and fully-localized-limit extremes.[54]

Within these approximations, the LSDA+U correction to the LSDA potential is

$$\Delta V(mm'\sigma) = -(U-J)\left(\rho^{\sigma}_{mm'} - \frac{1}{2}\delta_{mm'}\right), \tag{1}$$

where m, m' are the orbital indices, σ is the spin index, and $\rho^{\sigma}_{mm'}$ is the orbital occupation matrix. The effect of the LSDA+U correction given by Eq. (1) is particularly transparent in the limit of diagonal $\rho^{\sigma}_{mm'}$ with orbital occupancies 1 or 0: Occupied orbitals experience a potential which is lower in energy by $(U-J)/2$ compared with the LSDA, and the potential for unoccupied orbitals is raised by the same amount.

In this study we varied U_{eff} from 0 to 6 eV for the Ru d states (the standard LSDA corresponds to a U_{eff}=0 eV). Structural optimizations were also performed within LSDA+U approximation, however, negligible structural changes compared with the LSDA were observed.

C. Self-interaction corrections

Our second approach for extending the treatment of the exchange and correlation is to correct for the spurious self-Coulomb and self-exchange interactions which arise within the LSDA, using the pseudo-SIC method.[55–57] These self-interaction errors are small for materials with delocalized electronic states, but can be significant in systems with lo-

calized electrons where the interaction of an electron with itself is large.

Since the SIC in a periodic extended system is not uniquely defined, many different methods have been proposed to remove SI in DFT calculations for solids (for a review see Ref. 58). The procedure followed in the pseudo-SIC method is to:

(1) Project the occupied Bloch states onto the basis of the pseudoatomic orbitals.

(2) Correct the Kohn-Sham potential for each Bloch state by the SIC for the pseudoatomic orbital weighted by the projection, and scaled to account for the relaxation energy.

Note that only the valence bands are corrected since the empty conduction bands, derived from orbitals where the occupation numbers are close to zero, are not self-interacting. This is in contrast to the LSDA+U method, in which the occupied bands are lowered in energy and the unoccupied bands raised. In principle, however, the two formalisms would yield equivalent results if a suitable $U-J$ (corresponding to the SIC energy) were applied to all orbitals in the LSDA+U calculation. Indeed, whether the deficiencies of LSDA for strongly correlated systems derive from the absence of Hubbard U or the self-interaction error or both remains an open question. The pseudo-SIC method has some advantages over LSDA+U, since it does not require a choice of which orbital to correct, nor of the U or J parameters, and it can be applied readily to both magnetic and nonmagnetic systems. We note that this is the first application of pseudo-SIC to an itinerant-correlated system, so the comparison with our LSDA+U results provides a test for the pseudo-SIC method.

IV. RESULTS AND DISCUSSIONS

As we have mentioned, the electronic structure of $SrRuO_3$ has been investigated previously using the LSDA.[22,28,32] Here we first revisit the LSDA with our own calculations, with an emphasis on understanding discrepancies between the experimental measured photoemission results[18,19] and the calculated LSDA electronic structure of the orthorhombic material. We then extend our study to the two "beyond-LSDA" approaches to examine correlation effects in *bulk* *Pbnm* and $Pm\bar{3}m$ $SrRuO_3$. Finally, we examine unsupported *films* of $SrRuO_3$ in both structures in order to analyze the nature of the experimentally observed metal-insulator phase transformation.

A. Cubic LSDA

The total energies were calculated for both the ferromagnetically ordered and nonmagnetic states of cubic $SrRuO_3$ using the optimized lattice parameters. With both electronic structure codes the ferromagnetic ground state is always found to be lower in energy (VASP: by 11.5 meV, SIESTA: by 31.6 meV). Both codes yield very similar electronic structures. The density of states (DOS) obtained using the VASP code is shown in Fig. 2. The valence band is composed largely of O 2p states hybridized with Ru 4d states, with oxygen states predominately found in lower regions of the valence band and Ru states dominating at the Fermi energy. The large peak in the DOS near the Fermi level is caused by the fairly flat Ru t_{2g} bands near the Fermi level while the strongly hybridized e_g orbitals form broader bands at the bottom of the valence and conduction bands. The Sr 4d states are found around 5 eV above the Fermi energy.

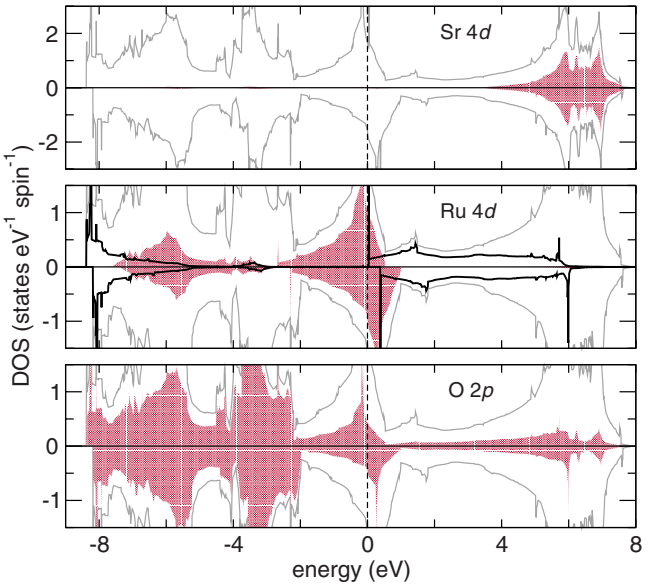

FIG. 2. (Color online) The total (gray line) and partial (shaded) spin-resolved densities of states for cubic $SrRuO_3$ calculated within the LSDA using VASP. (Upper) Sr 4d states, (middle) Ru 4d states [the t_{2g} and e_g (unshaded bold line) symmetries are shown], and (lower) O 2p states. The dashed line at 0 eV denotes the Fermi level.

The exchange splitting causes an energy shift between the majority spin and minority spin states; at the Γ point a splitting of $\approx$0.50 eV is observed in the Ru 4d states, and of $\approx$0.20 eV in the O 2p states. The calculated magnetic moments per formula unit are found to be 1.09 μ_B (VASP) and 1.26 μ_B (SIESTA). With both implementations of DFT, approximately 70% of the moment is found on the Ru atoms, with the remaining distributed on the oxygen network. The slight enhancement of the magnetic moment calculated with SIESTA compared to VASP is due to SIESTA's slight downward shift in energy of the Ru t_{2g} band relative to the Fermi energy. We note that the consistency between the two DFT flavors is essential to our later discussion of the effect of electron-electron correlations in the electronic structure of $SrRuO_3$, since the LSDA+U approach has been implemented in the VASP code, and the pseudo-SIC method in the SIESTA code.

B. Orthorhombic LSDA

Using the optimized LSDA lattice parameters for the *Pbnm* structure, we find that the ferromagnetic ground state is 6.34 meV/f.u. lower in energy than the constrained paramagnetic structure, and additionally is 188 meV/f.u. (VASP) and 150 meV/f.u. (SIESTA) lower in energy than the ferromagnetic cubic phase. This energy stabilization can be associated with the oxygen octahedral tiltings and rotations, and

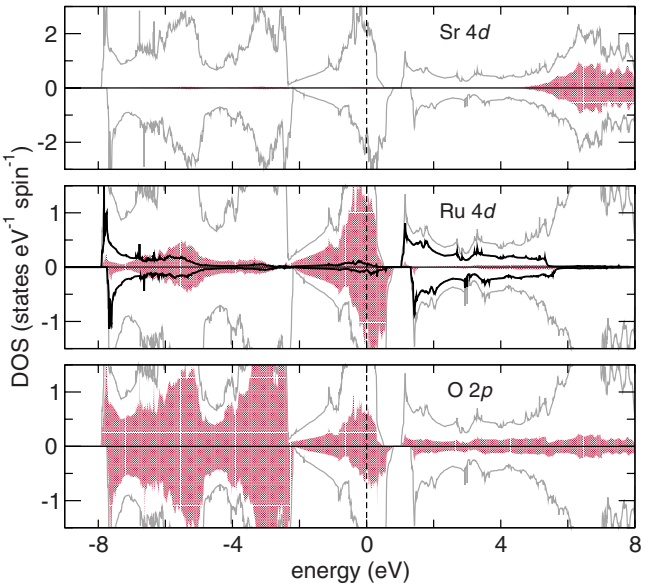

FIG. 3. (Color online) The total (gray line) and partial spin-resolved (shaded) densities of states for orthorhombic $SrRuO_3$ calculated within the LSDA using VASP. (Upper) Sr 4*d* states, (middle) Ru 4*d* states [the t_{2g} and e_g (unshaded bold line) symmetries are shown], and (lower) O 2*p* states.

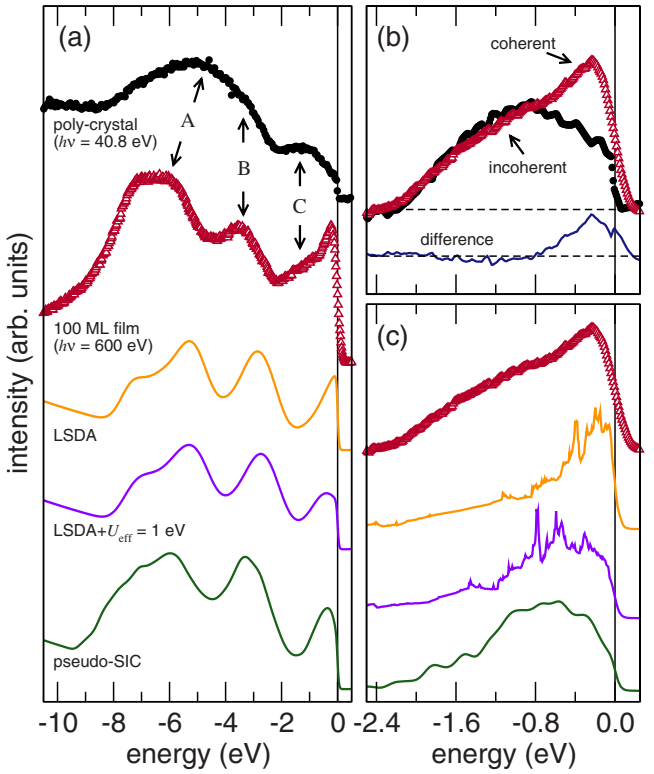

FIG. 4. (Color online) (a) The experimental PES spectra for bulk polycrystalline (Ref. 64) $SrRuO_3$ (filled circles) and 100 monolayer SRO film (Ref. 65) (triangles) grown on $SrTiO_3$ are compared to the calculated LSDA(+*U*) and pseudo-SIC densities of states. The calculated DOSs are broadened with an energy-dependent Lorentzian (FWHM=$0.1|\epsilon-\epsilon_F|$eV) and a Gaussian function (0.34 eV FWHM). An energy-dependent parabolic background has also been added. (b) Comparison of the experimental Ru 4*d* spectra resolved by subtracting a Gaussian function fitted to the O 2*p* contribution to the PES spectra. (c) Comparison of the thin film Ru 4*d* states to the calculated densities of states without additional broadening.

agrees well with previous first-principles studies[28,32] that used experimental lattice parameters[59] (the LSDA underestimates the lattice parameters by only about 1%). Also it is consistent with the experimental observation of ferromagnetic $SrRuO_3$ in the distorted $GdFeO_3$ structure.[59]

The (P)DOSs for the orthorhombic structure are shown in Fig. 3, and can be seen to be similar to those of the cubic structure discussed earlier (Fig. 2).[60] Consistent with the reduction in Ru 4*d*-O 2*p* overlap resulting from the tiltings and rotations, the bandwidths are slightly narrower in the orthorhombic structure, with the t_{2g} bandwidth reduced by 0.35 eV, the e_g by 1.5 eV, and the O 2*p* by 0.60 eV. This results in a pseudogap opening in the minority e_g bands at ≈ -2.2 eV and a 0.20 eV gap opening ≈ 0.80 eV above the Fermi level. Interestingly, the Ru 4*d* exchange splitting is reduced slightly at Γ. This is accompanied by a reduction in the magnetic moment compared with the cubic structure, to 0.79 μ_B/f.u. (VASP) or 0.92 μ_B/f.u. (SIESTA). As noted, the spontaneous magnetization in the bulk (films) has been reported to be near 1.1 μ_B (1.4 μ_B) (Ref. 61); the LSDA underestimate is likely the result of the usual LSDA overbinding leading to enhanced Ru 4*d*-O 2*p* covalency. In fact, because the orbital angular momentum is expected to be strongly quenched for 4*d* orbitals due to the cubic crystal field, this reduction in the local moment is rather interesting. We comment on the effect of including spin-orbit coupling later.

Finally for the LSDA section, we compare our first-principles LSDA results with recent PES data[20,62,63] with the goal of identifying which features are driven by correlation. In an ideal single-electron picture, the measured PES would consist of narrow peaks corresponding to the energies required to excite noninteracting electrons from the valence band into the continuum. However, the photoemission energies are more accurately interpreted as differences between two many-body *N*-electron states: the ground state, and the excited state with a photoelectron and hole. The effect of the many-body interactions is to broaden the one-electron peaks and shift spectral weight into so-called quasiparticle peaks. The strongest reduction in spectral weight from correlation effects occurs from so-called coherent peaks near ϵ_F, and is accompanied by transfer of the spectral weight to higher energy features (incoherent peaks). Redistribution of the incoherent spectral weight into a well-defined satellite structure is indicative of strong correlations, whereas a redistribution into the background spectral distribution with a renormalization of the bandwidth indicates weak correlations.

In Fig. 4(a), we show two experimentally measured spectra (see Refs. 18 and 64 for further information on the sample preparation) and our calculated LSDA results. Before commenting on the discrepancies between the bulk polycrystalline spectrum and that of the thin film, we point out that both spectra are dominated by three principle features (with the caveat that the bulk spectrum is highly broadened), which are assigned to different electronic states by comparing to

our calculated densities of states. In order to make this comparison, we convolute an energy-dependent Lorentzian function [full width at half maximum (FWHM)= $0.1|\epsilon-\epsilon_F|$eV)] with the calculated DOS to account for lifetime broadening. A Gaussian function with a FWHM=0.34 eV is also used to account for the instrumental resolution, and an energy-dependent parabolic background is also added. The O $2p$ bonding states are located between −8 and −5 eV (A), while the O $2p$ nonbonding states are found around 3.5 eV (B). In the range between −8 eV up to the Fermi level there are the occupied Ru $4d$ states, with the t_{2g} state lying across the Fermi energy beginning at −3 eV with a broad shoulder (C) between −2.4 and −0.7 eV.

In Fig. 4(b), we show more clearly the Ru $4d$ states around the Fermi level by removing the background intensity and the contribution of the O $2p$ states by fitting a Gaussian function to the experimental spectral distribution. In the thin film sample, the sharp coherent feature located below the Fermi level is broadened by the many-body effects already described; however an additional shoulder appears between −2.4 and −0.7 eV. This subtle spectral feature is a signature of correlation and is primarily due to spectral weight transfer from the coherent to the incoherent feature. On the other hand, the bulk polycrystalline sample shows only a single broad feature centered at −0.8 eV, with reduced spectral weight below the Fermi level. The question that one needs to answer before proceeding is whether or not this broad feature is due to intrinsic correlations or due to sample preparation techniques. Based on previous experimental comparisons between $SrRuO_3$ films and polycrystals,[66,67] this shift in the spectral weight to the incoherent peak is attributed to the creation of near surface states induced during *in situ* scraping and not due to intrinsic correlation effects. Additionally the presence of grain boundaries and compositional defects are also known to yield reduced coherent peak features in polycrystalline samples. We therefore restrict our comparison of the PES data to the 100 monolayer film for the remainder of this study, since it more accurately describes the intrinsic electronic structure.

Some important discrepancies exist between our LSDA results and the spectroscopic data: the Sr $4d$ states are positioned approximately 1.5 eV lower in energy than is expected from the experimental spectra as determined in the bremsstrahlung isochromat spectroscopy (BIS) and x-ray absorption spectroscopy (XAS) spectra (not shown).[20,62] The spread of the O $2p$ states is also underestimated. The most drastic difference, and one examined many times in the literature, occurs in the Ru $4d$ states, where indications of correlations are found. In Fig. 4(c), we show only the Ru $4d$ states near ϵ_F compared to our calculated densities of states (without broadening). As mentioned, the signature of strong correlations as observed in the PES data is the strong renormalization (or even absence) of the quasiparticle peak near ϵ_F or large satellite peaks. In the thin films, the weak coherent t_{2g} peak centered about 0.5 eV below the Fermi level has a substantial incoherent feature near −1.2 eV and is good evidence for localized electronic states from strong correlation effects. Experimentally the Ru $4d$ spectrum shows a coherent peak that is approximately 0.40 eV broader than the LSDA predicts. Furthermore, the incoherent feature in the experimental PES is 1.0 eV broader than in the LSDA calculation, where it is suppressed. The long tail in the t_{2g} states is likely due to hybridization with the nonbonding O $2p$ states.

More recent ultraviolet photoemission spectroscopy (UPS) data[21] suggest that the Ru stoichiometry plays a significant role in determining the spectral weight and intensity of the t_{2g} peak at the Fermi level. For stoichiometric $SrRuO_3$ films, the spectral intensity near the Fermi level is in much better agreement with the calculated PDOS, while Ru deficient samples have a reduced intensity. These facts suggest that previous comparisons may have been made with nonstoichiometric Ru samples, which may be caused by a high partial pressure of oxygen during growth. Although the Ru cation deficiency appears to explain the discrepancy with experimentally measured spectra, it is difficult to fully remove correlation effects that implicitly result from changes in stoichiometry, e.g., the d bandwidth can be varied by changing the volume of the unit cell via changes in O-Ru-O bond angles which occurs upon Ru vacancy formation. For example, Siemons and co-workers[21] found the enhancement of an incoherent peak at approximately 1.5 eV below the Fermi level in ruthenium poor samples measured with ultraviolet photoemission spectroscopy. Future first-principles calculations may be able to identify the role of these defects.

It is clear that the LSDA incompletely describes the electronic and magnetic structure of bulk $SrRuO_3$, and this suggests that some underlying physics may be missing in the local spin-density approximation. We next explore two extensions of that description to address whether the incoherent feature missing in the LSDA calculations, as well as the reduced magnetization, could be due to correlated electron-electron interactions, and whether these can be captured by a static on-site correction.

C. "Beyond LSDA"

We now explicitly add correlation effects into our electronic structure calculations for $SrRuO_3$ using the two methods outlined above. The pseudo-SIC and LSDA+U methods give very similar results when a U_{eff}=1.0 eV is used. Therefore we first compare the correlated and LSDA results, and later point out the small differences between results from the two correlated formalisms.

1. Orthorhombic

Figure 5 shows the densities of states calculated with LSDA+U with a U_{eff}=1.0 eV and the pseudo-SIC method for *Pbnm* $SrRuO_3$. Compared with the LSDA, the correlated bands are narrower, with energy gaps appearing in both spin channels. The inclusion of correlations causes a 70% drop in the total DOS at the Fermi level compared with LSDA, with the result that the contribution to the Ru $4d$ states is almost entirely derived from the minority spin channel, and the material is close to half-metallicity. This significantly enhances the magnetic properties compared to the LSDA, increasing the magnetic moment per formula unit to around 1.9 μ_B (Table III), and enhances the exchange splitting of the Ru $4d$ states at Γ to 0.45 eV ($\approx$0.30 eV in LSDA). In addition, the

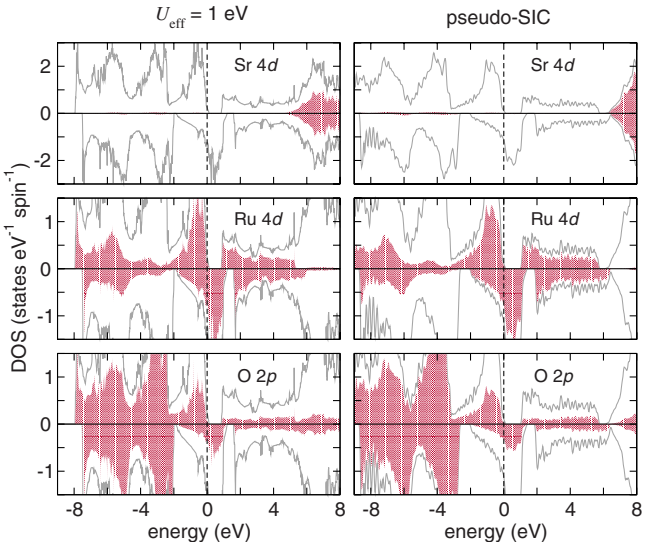

FIG. 5. (Color online) The total (gray line) and partial spin-resolved (shaded) density of states for orthorhombic $SrRuO_3$ calculated with U_{eff}=1 eV (left) and pseudo-SIC (right) are shown in each panel. (Upper) Sr 4*d* states, (middle) Ru 4*d* states, and (lower) O 2*p* states.

peak positions of the correlation-included densities of states are in better agreement with the experimental spectra [Fig. 4(a)], although the intensity of the O 2*p* peak at ≈−7 eV is still low compared with that of the Ru t_{2g} peak.

The main difference between the electronic structures calculated with U_{eff}=1 eV and the pseudo-SIC methods is a larger bandwidth of the occupied orbitals, by ≈1.7 eV, in the pseudo-SIC calculation. This has the greatest effect on the Ru 4*d* bands and the oxygen 2*p* bands near −8.0 eV. As a result, the pseudo-SIC shows better agreement with the PES in the bandwidth for the O 2*p* states between −8 and −4 eV, and as a result reproduces more closely the correct ratio of the higher energy features to the Ru the t_{2g} peak. In Fig. 4(c) it is clear that both the LSDA+*U* method and the pseudo-SIC suppress the t_{2g} states at the Fermi level and shift the center to higher energy (near −0.6 eV). However, the pseudo-SIC more accurately reproduces the incoherent feature found experimentally at −1.2 eV when compared to the LSDA+*U* result, while still maintaining a defined coherent peak.

In order to understand how the hybridization changes as electron-electron correlation effects are included, we plot in Fig. 6 the change in bandwidth for the Ru 4*d* and O 2*p* states

TABLE III. Summary of the calculated magnetic moments given in μ_B compared to the available experimental data. Values followed by a star (*) are calculated with the SIESTA code.

	Orthorhombic	Cubic
Experimental	0.90–1.60	*n*/*a*
LSDA	0.79	1.09
	0.92*	1.26*
LSDA+U_{eff}=1 eV	1.97	1.64
Pseudo-SIC	1.99*	1.77*

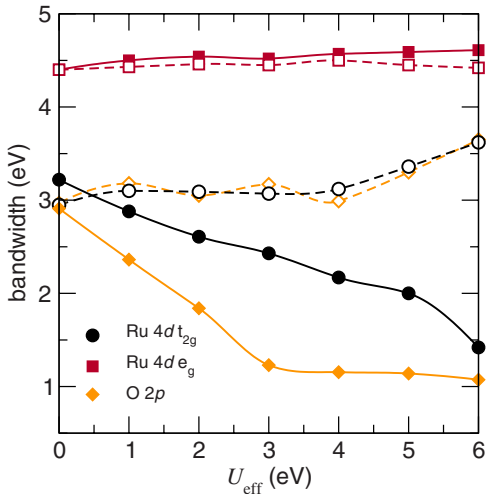

FIG. 6. (Color online) The orbital bandwidth dependence on U_{eff} for orthorhombic $SrRuO_3$. The minority spin states are shown by the unshaded symbols and the lines are a guide for the eyes. Using the pseudo-SIC method, the majority (minority) bandwidths are slightly larger than with the LSDA+*U* method, but the relative ratios are consistent: Ru 4*d* t_{2g}=3.30 (3.50) eV, Ru 4*d* e_g=4.75 (4.60) eV, and O 2*p*=3.25 (3.50) eV.

as a function of U_{eff} for orthorhombic $SrRuO_3$. As the amount of correlation is increased in the calculation through the U_{eff} term, the majority Ru t_{2g} and O 2*p* bandwidths are strongly reduced, and upon narrowing (both by approximately 1.80 eV) half-metallic behavior is observed for U_{eff} >2 eV. On the other hand, only a weak dependence in the orbital bandwidth is observed for the minority spin states. The valence bandwidth never narrows sufficiently in the bulk material (due mostly to the insensitivity of the minority t_{2g} bands to correlation effect) to open an insulating gap in both spin channels.

Since the half-metallic ground state that we find for U_{eff} >2 eV is not observed experimentally, and motivated also by the observation of large magnetic anisotropy in Kerr rotation measurements[68] on $SrRuO_3$ we have repeated our calculations with spin-orbit coupling (SOC) effects included. In Fig. 7 we plot the band structure along Γ−*X* in the Brillouin zone as a function of increasing U_{eff}. We see that the t_{2g} bands move down in energy with increasing U_{eff}, forming a small hole pocket which becomes completely filled at U_{eff} =2 eV giving the half-metallic behavior. We note that without careful sampling of the Brillouin zone, this hole pocket is often missed, and half-metallic behavior can be prematurely predicted. Furthermore, we superimpose the band structure calculated with U_{eff}=2 eV and spin-orbit coupling in Fig. 7. We find here that the degeneracy of the t_{2g} bands is completely removed, and the highest occupied majority band is pushed only 0.05 eV higher in energy. Furthermore, this splitting decreases at larger U_{eff} values. These results indicate that the inclusion of spin-orbit coupling does not have a large effect on the band structure. Although spin is strictly not a good quantum number, due to quenching of the angular momentum by the crystal field, the total angular momentum is well approximated by the spin-only component, and therefore the calculated proximity to half-metallicity in $SrRuO_3$ is robust to spin-orbit coupling effects.

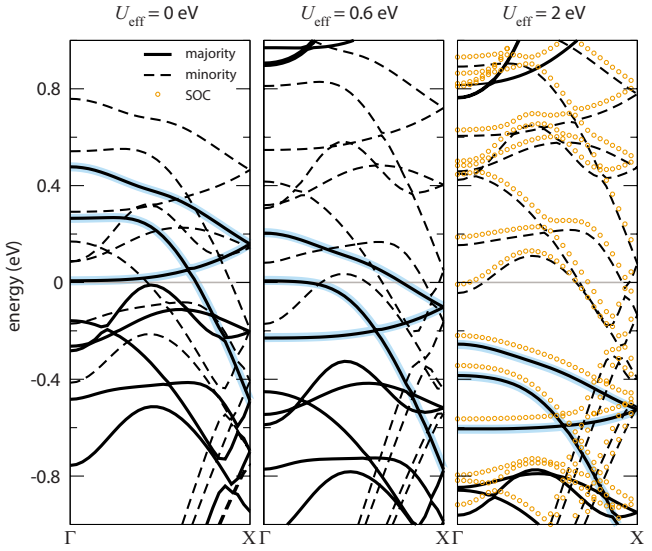

FIG. 7. (Color online) LSDA+U band structures along $\Gamma-X$ calculated with VASP for ferromagnetic orthorhombic $SrRuO_3$. The horizontal gray line marks the Fermi level. Majority (minority) bands are shown as the bold (dashed) lines. The highlighted bands indicate the filling of the majority t_{2g} hole pocket, which gives rise to the observed half-metallicity at large Hubbard U values. For U_{eff}=2 eV, the open circles show the results of calculations including spin-orbit coupling.

Finally we investigate the enhancement of the magnetic properties as U_{eff} is increased. In Fig. 8 (inset) we show the magnetic moment per formula unit as a function of increased correlation for both crystal structures of $SrRuO_3$. For example, the magnetic moment per Ru atom is found to be 1.97 μ_B with U_{eff}=1.0 eV and 1.99 μ_B with the pseudo-SIC (Table III). At $U_{eff} \geq 2$ eV saturation of the moment occurs, and the localized ionic moment is observed (2.0 μ_B).

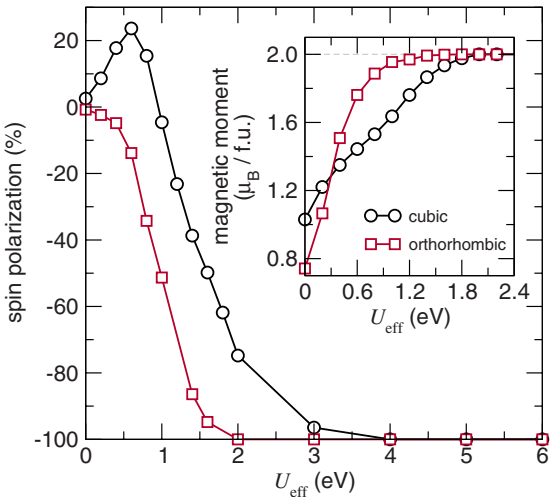

FIG. 8. (Color online) Calculated spin polarization at the Fermi level ($P_0^{\epsilon_F}$) for orthorhombic and cubic $SrRuO_3$ calculated with VASP as a function of U_{eff}. The pseudo-SIC calculations give a spin polarization of +2.0% and 8.8% for each structure, respectively. (Inset) Calculated magnetic moment per formula unit for each structure type with LSDA+U. The pseudo-SIC calculations yield a magnetic moment of 1.99 and 1.77 μ_B/f.u. for each structure, respectively.

2. Cubic

We complete this discussion by describing the differences in the bulk cubic electronic structure with correlation effects added in order to isolate the contribution of the octahedral distortions in the orthorhombic structure to the bandwidth narrowing. This analysis will provide the framework for exploring the MI transition in the $SrRuO_3$ thin films. Overall the weight and shape of the total density of states with correlations included are consistent with that calculated in the LSDA, with the exception that the large densities of states at the Fermi level (majority t_{2g} states) are pushed lower in energy. As was observed in the orthorhombic structure, a similar DOS is found between both correlation methods, and in general the occupied orbitals with the pseudo-SIC are broadened by 1.5 eV in energy compared to those calculated with the LSDA+U. As in the orthorhombic structure the minority bandwidths in the cubic case are insensitive to the choice of U_{eff} while the majority O $2p$ and Ru t_{2g} bandwidths narrow considerably (1.2 and 1.8 eV, respectively). Furthermore, the observed exchange splittings for the various states are overall larger for the cubic structure, and this is consistent with the electronic structures calculated with the LSDA. The calculated magnetic moment for U_{eff}=1 eV is 1.64 μ_B and agrees well with that from the pseudo-SIC method (1.77 μ_B). Again, for values of $U_{eff}>2$ eV a half-metallic ground state becomes stable while with the pseudo-SIC a fully metallic ground state is always maintained.

To summarize the bulk $SrRuO_3$ results, each of the two "beyond-LSDA" methods described here improves the description of the electronic and magnetic structure. However the precise experimental spectra are not fully reproduced although correct peak assignments can be made. The addition of a small Hubbard term U_{eff}=0.6 (1.2) eV for the orthorhombic (cubic) structure, or alternatively by correcting the SI error in LSDA, also improves the Ru t_{2g} bandwidths with respect to experiment.[26] The total width of the O $2p$ band structure is also increased to approximately 7 eV in agreement with the spectral weights. We therefore suggest that $SrRuO_3$ can best be described as moderately correlated. Finally, as stated earlier, the intensity at ϵ_F has been decreased in comparison to LSDA, although it is still larger than experimentally observed.

D. Spin polarization and transport properties

$SrRuO_3$ has been experimentally reported[69] to belong to the class of negatively spin-polarized materials—characterized by a greater number of *minority* spins at the Fermi surface which are aligned antiparallel to the bulk magnetization. However, the magnitude of the spin polarization at the Fermi level remains controversial within the experimental community, due in part to the different definitions of the spin polarization (resulting from the different experimental techniques used to probe this quantity), as well as to difficulties in performing the experiments. Furthermore, the theoretical community has also not converged on the magni-

tude of the spin polarization, due to the sensitivity of the Ru t_{2g} states near ϵ_F on the choice of exchange-correlation functional. In this section, we perform first-principles transport calculations on orthorhombic and cubic $SrRuO_3$, and compare our results to the available data in the literature. We also describe the various definitions of the spin polarization commonly used in the literature, and relate them to calculated *ab initio* quantities.

The spin polarization at the Fermi level $P_0^{\epsilon_F}$ can be calculated from the density of states at the Fermi level (N_{ϵ_F}) by the following ratio:

$$P_0^{\epsilon_F} = \frac{N_{\epsilon_F}^{\uparrow} - N_{\epsilon_F}^{\downarrow}}{N_{\epsilon_F}^{\uparrow} + N_{\epsilon_F}^{\downarrow}}. \tag{2}$$

Using this definition with the LSDA, the sign of the spin polarization for orthorhombic $SrRuO_3$ is ambiguous: we find that with the plane-wave code $P_0^{\epsilon_F} = -2.95\%$ while the local orbital code gives a positive spin polarization of 2.00%. In contrast, for the cubic structure we find a positive spin polarization ($P_0^{\epsilon_F}$) in both first-principles calculations, +1.3% (VASP) and +8.8% (SIESTA). The reason for this discrepancy is the sensitivity of the exchange splitting of the Ru 4*d* bands near the Fermi level to the structure. The majority t_{2g} band is positioned very close to the band edge, and its precise location is sensitive to the finer details of the DFT calculation. As a result, the large spread in the calculated spin polarization is not surprising, and since the magnitudes of the spin polarizations are small, changes of a few percent can give a change in sign.

When correlations are introduced, $P_0^{\epsilon_F}$ increases in magnitude significantly and is negative in all cases. The spin polarization as a function of U_{eff} for the orthorhombic and cubic structures is plotted in Fig. 8. The spin polarization calculated for the orthorhombic structure with the pseudo-SIC method is −85.7%, compared with a value of +2.00% when the SI error is not corrected. This value agrees with that obtained by the LSDA+U when $U_{\text{eff}}=1.4$ eV. We previously found that smaller U_{eff} values optimize the agreement between pseudo-SIC and LSDA+U band structures and magnetic properties, suggesting that the pseudo-SIC transport results should be regarded as providing an upper bound on the magnitudes of spin polarization. For U_{eff} exceeding a critical value of 1.6 eV (3.0 eV) the half-metallic ground state becomes the most stable solution for orthorhombic (cubic) structure, as an energy gap opens in the majority t_{2g} band and $P_0^{\epsilon_F}$ reaches 100%.

Despite being the most natural definition of spin polarization at the Fermi level, determining $P_0^{\epsilon_F}$ as defined in Eq. (2), is a nontrivial experimental process, since the spectroscopic measurements required typically have poor energy resolution. As knowledge of the degree of spin polarization in a ferromagnet is crucial for its use in spintronics, several different experimental methods have been developed in order to determine this quantity.

The *transport* spin polarization can be defined as

$$P = \frac{I^{\uparrow} - I^{\downarrow}}{I^{\uparrow} + I^{\downarrow}}, \tag{3}$$

where I^{σ} is the spin-dependent current. However I^{σ} is not directly observable and must be determined indirectly. The transport spin polarization now depends on the experiment in question, and in particular whether the transport is in the ballistic or diffusive regime. In the ballistic limit the current is proportional to $N_{\epsilon_F}\nu_F$, while for diffusive transport it is proportional to $N_{\epsilon_F}\nu_F^2$ (assuming both spin species have the same relaxation time), where ν_F^{σ} are the spin-dependent Fermi velocities.

Therefore the transport spin polarization at the Fermi level can be redefined as

$$P_n^{\epsilon_F} = \frac{N_{\epsilon_F}^{\uparrow}\nu_F^{n\uparrow} - N_{\epsilon_F}^{\downarrow}\nu_F^{n\downarrow}}{N_{\epsilon_F}^{\uparrow}\nu_F^{n\uparrow} + N_{\epsilon_F}^{\downarrow}\nu_F^{n\downarrow}}, \tag{4}$$

where $n=1$ for ballistic transport or $n=2$ for diffusive transport.[70,71] If $n=0$, this definition reduces to that of the spectroscopic polarization, $P_0^{\epsilon_F}$.

An additional definition of polarization is used in Meservey-Tedrow style tunneling experiments. Here the spin-dependent DOSs are weighted by their corresponding tunneling matrix elements. Such an experiment has been performed for SRO and report approximately a −10% spin polarization.[69] Inverse tunnel magnetoresistance measurements also agree that SRO is negatively spin polarized.[2] This is in agreement with the majority of the calculations which find that SRO is a negatively spin-polarized material at the Fermi surface.

The point-contact Andreev reflection (PCAR) technique, which is based on the process of Andreev reflection[72] and developed as an experimental method in the work of Soulen *et al.*[73] and Upadhyay *et al.*,[74] has been used successfully to determine the magnitude of the transport spin polarization, although it is not sensitive to its sign. Experimental results[75–77] using this method report values ranging between 51% and 60%. It should be noted that in the Andreev experiment the polarization is not uniquely defined, in that it must be extracted from the data through a fitting procedure and involve terms that describe the transmittivity of the interface between the ferromagnet and the superconductor. These parameters are typically difficult to determine precisely and consequently introduce further uncertainty in the experimental spin polarization. Furthermore, it is important to note that in all PCAR experiments, it is necessary to establish whether the transport is in the ballistic, diffusive or intermediate regime (noninteger n) which ultimately depends on the transmittivity of the interface. The experimental results for SRO are further complicated by the fact that the transport in the system has been measured in both regimes.

To allow for a direct comparison with the PCAR experiments, the transport spin polarization in both the ballistic and diffusive limit was determined using the *ab initio* electronic transport code SMEAGOL.[78] Here we calculated the transport at zero bias through both the orthorhombic and cubic structures,[79] and present the results in Table IV and Fig. 9. The shortcomings of the LSDA in describing the spin polarization at the Fermi level in $SrRuO_3$ are again apparent. The highest spin polarization obtained with the LSDA for the orthorhombic structure is −15% and it is obtained in the

TABLE IV. Transport spin polarizations calculated with SMEAGOL, according to the definition of Eq. (4) using both the LDSA and pseudo-SIC. Results for both the orthorhombic and cubic $SrRuO_3$ structures are included.

	Orthorhombic	Cubic
	$P_n^{\epsilon_F}$ % (LSDA, pseudo-SIC)	
$n=0$	+2.00,−85.7	+8.80,−16.1
$n=1$	−1.44,−92.9	−8.99,−50.9
$n=2$	−15.1,−98.0	−32.9,−79.5

diffusive limit. This is notably smaller than the experimental PCAR results measuring the same quantity, $P_2^{\epsilon_F}$. As shown in Fig. 9, on changing from $P_0^{\epsilon_F}$ to $P_2^{\epsilon_F}$ the polarization increases and becomes more negative. Since the group velocity tends to zero at the band edge, and is often maximized at the band center, higher powers of n in $P_n^{\epsilon_F}$ suppress the contribution of the Ru 4*d* states at the band edge while enhancing those at the band center. From Fig. 9 it is then clear that the large negative polarization is a consequence of the center of the *majority* Ru 4*d* band positioned approximately 1 eV below the Fermi level, while the *minority* Ru 4*d* band center is aligned across the Fermi level.

Further enhancement is seen by introducing correlation; for example, by correcting for the SI error, the spin polarization increases due to the reduction in the number of majority Ru t_{2g} states at the Fermi level. The correlated *ab initio* calculations now give very high spin polarization, ranging between −85.7% and −98.0%, whereas the highest value achieved experimentally is just 60%. Qualitatively similar results are found for the cubic structure, although the SIC in general has a smaller influence on the spin polarization. For example, $P_1^{\epsilon_F}$ goes from −8.99% (LSDA) to −50.9% (pseudo-SIC), while $P_2^{\epsilon_F}$ goes from −32.9% to −79.5%.

It is also useful to note the strong dependence of spin polarization on distance from the Fermi level. In Fig. 10 we show for the orthorhombic structure that if the Fermi level is moved just 100 meV into the valence band, $P_1^{\epsilon_F}$ is decreased to −81.4%, while moving E_F by −200 meV decreases it further to −59.8%, bringing it within the experimental range of values. In practice this shift in the Fermi level can be realized

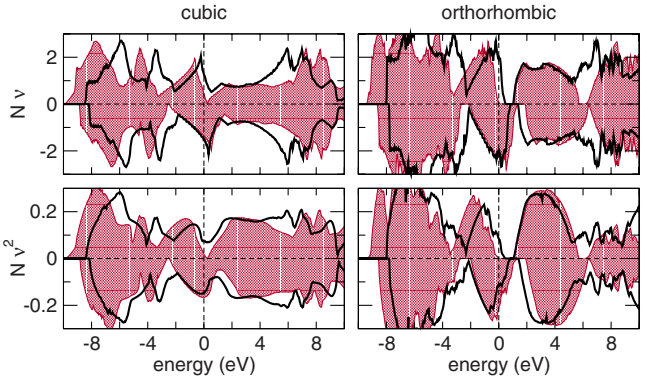

FIG. 9. (Color online) Spin-dependent transport coefficients, $N\nu$ and $N\nu^2$, calculated with both the LSDA (unshaded) and pseudo-SIC (shaded).

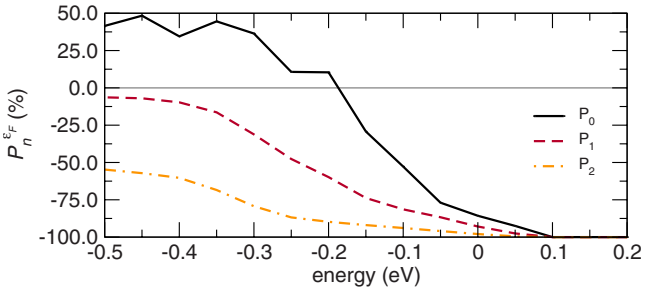

FIG. 10. (Color online) Spin polarization defined according to Eq. (4) as a function of distance from the Fermi energy (set to 0 eV) and calculated with the pseudo-SIC for the orthorhombic structure.

by off-stoichiometric compounds such as those investigated by Siemons *et al.*[21]

The discrepancy between the computational and experimental results could be then due to a number of factors: for example, there are several known limitations with PCAR including spin-flip scattering events which could drastically reduce the measured value of P^{ϵ_F}, as well as the possible ambiguous fit of PCAR measurements to a multiparameter model.[80] We also note that spin-orbit coupling, which we did not account for in our transport calculations, could reduce the spin polarization at the Fermi level.

Despite these disparities, both *ab initio* calculations and experiment show $SrRuO_3$ with a high negative spin polarization. As expected, LSDA underestimates the spin polarization at the Fermi level, whereas the inclusion of correlation through the correction of the SI error with the pseudo-SIC results in much better agreement between theory and experiment.

E. Thin films

The electronic and magnetic structure of epitaxially grown oxide multilayers can be tuned by controlling the film thickness. In particular, it has been demonstrated that metallic $SrRuO_3$ can be transformed into an insulating state by growing films thinner than five monolayers on $SrTiO_3$ substrates.[18] It was also found that the Curie temperature decreases with reduced film thickness, along with the disappearance of strong ferromagnetic order. Photoemission experiments show a shift in the spectral weight to the incoherent peak features in the spectra, suggesting that these effects are a result of changes in electron-electron correlation effects. With our first-principles techniques, we systematically investigate whether we can reproduce this transition purely from structural confinement, or by also including correlation effects and/or the octahedral tiltings of the orthorhombic structure. For the remainder of this section, we choose to include correlation with the LSDA+U method, rather than the pseudo-SIC method, and note that from the discussion so far, both methods reproduce similar electronic structures.

1. Cubic LSDA slabs

To investigate the effects of structural confinement on the metal-insulator transition, we first performed a series of slab

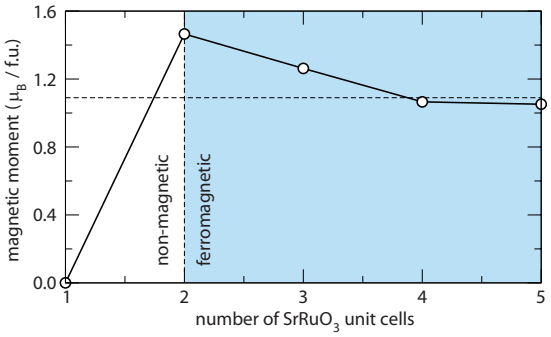

FIG. 11. (Color online) Magnetic moment dependence on slab thickness for cubic $SrRuO_3$. The bulk LSDA magnetic moment is shown as the dashed line. The total energy differences are calculated for the spin-polarized films with respect to the nonmagnetic ground state.

calculations (from 1 to 5 unit cells thick) on cubic $SrRuO_3$ constrained to the calculated bulk equilibrium $SrTiO_3$ lattice parameter. This is in part motivated by the fact that good epitaxy is made with the substrate surface, and that tilting of the octahedra may be suppressed. Additionally, it is computationally more feasible to systematically investigate these smaller supercell slabs. We will discuss later the effect of including the octahedra tiltings in the orthorhombic thin films; we saw earlier that this structural effect is important in fully describing the subtle details of the electronic structure of SRO. In all calculations the slabs were terminated with a SrO surface, to be consistent with that experimentally observed to be the most thermodynamically stable.[81]

In Fig. 11 we plot the Ru magnetic moment (per f.u.) as a function of increasing slab thickness. We find that the LSDA films become nonmagnetic below a critical thickness of only two monolayers; this is lower than the experimentally observed loss of the strong ferromagnetic order below six monolayers.[82] In addition, all of our calculations on the cubic films remain metallic down to one monolayer. Experimentally the situation is different and insulating behavior is observed in heteroepitaxial thin films at six monolayers on $SrTiO_3$. At one unit cell, where all atoms are surfacelike, the magnetic moment is considerably suppressed from its bulk value, and the nonmagnetic structure is actually lower in energy. An enhancement in the magnetic moment is observed at two unit cells in thickness; the moment then decreases toward the bulk value as the film thickness grows. For films larger than two unit cells, the ferromagnetic ground state is always found to be stable. In a mean-field theory approach, the energy difference between the ferromagnetic and the paramagnetic ground states Δ can be expected to be proportional to the Curie temperature T_c according to $k_B T_c = \frac{2}{3}\Delta$. For the four and five unit cell slabs, we find mean field T_c's of 170 and 120 K, respectively; these values are close to the experimental bulk value of 160 K suggesting that even in these thin films the strong itinerancy remains. This is consistent with temperature-dependent magnetization data recorded on strained and free standing films[83] as well as on ultrathin $SrRuO_3$ films.[82] Additionally, the spin polarization $P_0^{\epsilon_F}$ as a function of slab thickness (not shown) exhibits a large negative polarization at two unit cells, while a small positive spin polarization is found with increasing thickness (consistent with our bulk spin-polarization calculations). Most importantly, the insulating state is not found in any of the cubic slab calculations nor is the nonmagnetic ground state generally favored (the one unit cell case is an exception and is due to competing interactions from surface effects).

To better understand how the magnetism is distributed in the slabs, we have also calculated the layer-by-layer local density of states (LDOS). As in the bulk case, on average the majority of the spin ($\approx$65%) is located on the Ru atom, with the remaining found on the oxygen network. Interestingly, the Ru atoms closest to the surface layers experience a suppressed magnetic moment for each slab. This is in contrast to most transition-metal (nonoxide) ferromagnets, where often enhancement occurs due to a loss of coordination, weaker interatomic hybridization, and enhancement of the orbital angular momentum. In this oxide, enhanced covalency at the surface layer may be responsible for the reduced magnetism.

Before adding correlation effects in the cubic slabs, we first discuss the changes in the electronic structure due to the thin film geometry. The overall shape and weight of the density of states for the cubic slab and the bulk cubic LSDA calculation are very similar suggesting that confinement effects are minimal. The calculated exchange splittings are also similar with the exception that the Ru 4*d* states are split by approximately 0.25 eV. A small gap in the minority e_g states opens at approximately −4.30 eV, and partial occupation of the majority e_g states occurs; these features are not observed in the bulk cubic LSDA calculation. For a free standing, three-unit-cell film we find that the structure has a magnetic moment of 1.26 μ_B and a spin polarization of +13.2% within the LSDA, both larger than the bulk cubic values of 1.09 μ_B and +1.3%, respectively. The increased positive spin polarization is a result of the band center of the minority Ru 4*d* states shifting to higher energy in the thin films. To summarize the results for the cubic $SrRuO_3$ thin films, we do not find a metal-insulator transition as a function of film thickness, although we do find a slightly enhanced magnetization. We therefore are able to rule out the effect of dimensional confinement as the driving force for a metal-insulator transition.

2. Cubic LSDA+U slabs

We now examine the effect of adding correlation in the calculations for the cubic thin films in order to determine if electron-electron correlation in these structures is sufficient to obtain a metal-insulator transition. Here we use a $U_{\text{eff}} = 2$ eV, which although larger than that we described earlier to more accurately reproduce the PES spectra, does allow us to verify that in the absence of insulating behavior, the driving force for the MI transition is not due to intrinsic correlation effects. Although the numbers we discuss here are particular to a three-unit-cell thin film we note that the general trends are consistent across the series of cubic thin films. In contrast to the LSDA calculations, when a finite Hubbard U is placed on the Ru 4*d* states, we find that the majority e_g states are completely unoccupied, and occupation of the majority O 2*p* states near −2.3 eV is enhanced over the minority O 2*p* states which nearly open a gap in the minority spin

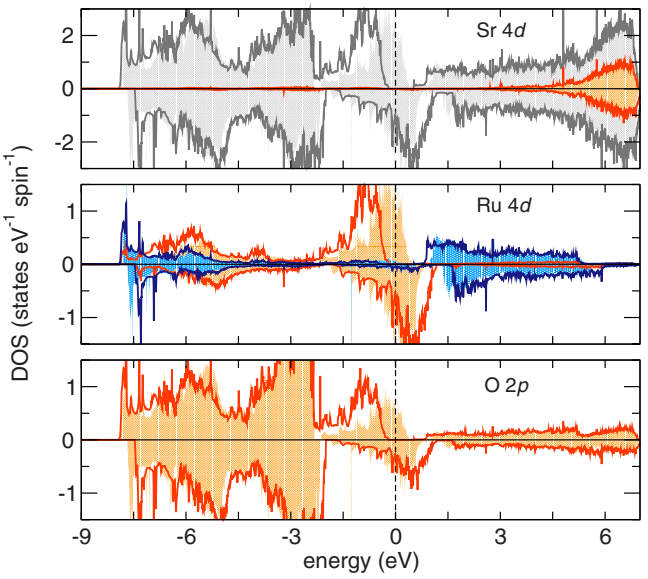

FIG. 12. (Color online) The total and partial spin-resolved density of states for a three-unit-cell orthorhombic $SrRuO_3$ slab calculated with $U_{\text{eff}}=0$ eV (shaded) and $U_{\text{eff}}=2$ eV (unshaded, bold) are shown in each panel. (Upper) Total (gray) and Sr 4*d* states, (middle) Ru 4*d* states, t_{2g} and e_g, and (lower) O 2*p* states.

channel. An enhancement in the exchange splitting for the Ru *d* orbitals is also observed with $U_{\text{eff}}=2$ eV compared to $U_{\text{eff}}=0$ eV, while the valence bandwidth is reduced. For the cubic slab with $U_{\text{eff}}=2$ eV, the narrowing of the bandwidth nearly stabilizes a half-metallic ground state, as the majority Ru t_{2g} bands become completely filled. Despite these small changes in the occupation of the Ru 4*d* levels, we do not find an insulating ground state in any of the cubic slabs even in the presence of strong correlations ($U_{\text{eff}}<6$ eV). Regarding the magnetic moment in these slabs, we find 2.0 μ_B/f.u. for $U_{\text{eff}}=2$ eV, and a corresponding spin polarization at the Fermi level of −85.9%. These results are consistent with the effects of adding correlation in bulk cubic $SrRuO_3$, and because an insulating ground state is not achieved, we suggest that neither correlations nor structural confinement (from our previous discussion) is sufficient to induce a metal-insulator transition.

3. Orthorhombic LSDA slabs

We now address films of orthorhombic $SrRuO_3$ which allow the full octahedral distortions found in the bulk experimental structure to occur. Earlier we showed that the effect of these distortions in the bulk is to reduce the t_{2g} valence bandwidth; in this section we examine whether these distortions with the addition of a confined geometry in a thin film form can stabilize the experimentally observed insulating $SrRuO_3$ ground state. With the relaxed coordinates for bulk *Pbnm* $SrRuO_3$, we calculate the electronic ground state for a three-unit-cell-thick slab separated by 10 Å of vacuum on each side and SrO termination layers within both the LSDA and LSDA+*U* method ($U_{\text{eff}}=2$ eV).[84]

We now discuss the changes in the electronic structure of the orthorhombic thin film: in Fig. 12 we show the (P)DOS for the three-unit-cell slab with and without correlation. With the LSDA in the thin film system, the exchange splittings are similar to the bulk LSDA orthorhombic calculations, and the character around the Fermi level remains a mixture of majority and minority Ru t_{2g}. Energy gaps similar to those found in the bulk are observed in other regions of the electronic structure with the exception that an additional gap opens in the minority t_{2g} states at −2.5 eV, which is not observed in the bulk calculation.

We now compare the magnetic properties of the LSDA slab calculation to the bulk *Pbnm* LSDA calculation. With the LSDA method, we find a magnetic moment of 1.01 μ_B per Ru atom and a spin polarization at the Fermi level of $P_0^{\epsilon_F}=-7.96\%$ (compared to a bulk orthorhombic structure with a moment of 0.79 μ_B and spin polarization of −2.95%). Therefore, we find enhanced magnetic properties in the thin film geometry when the octahedral tiltings are included. However we still do not find an insulating ground state.

4. Orthorhombic LSDA+U slabs

Finally we incorporate correlation into the orthorhombic slab calculations and examine the effect on the electronic and magnetic structure. We have already demonstrated that a $U_{\text{eff}}=2$ eV is sufficient to establish a half-metallic ground state in the bulk orthorhombic structure; therefore, we use this limit to establish whether correlation can drive the insulating ground state. If we do not find a metal-insulator transition even at this large Hubbard *U* value, we can be certain that the effect is not due to correlation. In general, the shape and weight of the densities of states and exchange splittings for the different states remain similar to the orthorhombic LSDA slab calculation, however unlike the cubic slabs, the valence bandwidth does not noticeably narrow.

With the addition of the Hubbard *U* term in the calculation, the half-metallic ground state becomes stable, with 0.70 eV energy gap opening in the majority spin states. This behavior is realized by the minority t_{2g} bands shifting higher in energy while the majority bands become completely occupied. The majority e_g band is also lowered in energy from 1.0 eV in the LSDA slab calculation ($U_{\text{eff}}=0$ eV) to 0.50 eV, while the minority spin states move 0.30 eV higher in energy with $U_{\text{eff}}=2$ eV. Similar energy gaps are observed as in the LSDA slab calculation, with the caveat that there is no gap in the majority O 2*p* states below the Fermi level; this is due to a shift of the O 2*p* states from the Fermi level to lower energy when correlation is added. With a $U_{\text{eff}}=2$ eV we find −100% spin polarization at the Fermi level and a magnetic moment of 2.0 μ_B per Ru atom. This effect on the magnetism with increased correlation is consistent with that found in the bulk calculations.

In summary, we never find a fully insulating ground state in our thin film calculations even in the presence of large correlation effects. We have also examined the layer-by-layer DOS for each slab (data not shown) and have not found an insulating surface layer in any of the calculations. However, as a result of the 2D confinement in the slabs, we do observe a narrowing of the minority t_{2g} bandwidth, and a shift of the Fermi level away from the band center. Furthermore, with correlations the Fermi level also is seen to cut across the

band edge. These two properties together indicate that $SrRuO_3$ thin films are closer to a metal-insulator instability (with regards to the bulk), and consequently disorder is more likely to induce electron localization and form an insulating state. From these results we suggest the following two possibilities regarding the experimentally observed metal-insulator transition: (1) either the transition in $SrRuO_3$ thin films is not an intrinsic property of the system, but rather extrinsic and possibly due to surface roughness or defects from film deposition combined with the band narrowing from confinement and correlation, or (2) that $SrRuO_3$ thin films must be treated with more exotic electronic structure methods.

It is worth mentioning that PES experiments[66] of $SrRuO_3$ films grown on $SrTiO_3$ substrates found a strong sensitivity of the t_{2g} spectral intensity and weight early in the deposition process (less than eight monolayers) with the intensity of the Ru 4*d* states becoming strongly enhanced above 15 monolayers. It was found that the film growth proceeds with a step terrace mechanism with minor atomic diffusion at less than five monolayers and followed by 3D island growth.[82] The disordered growth process should also reduce the stability of the ferromagnetic order, and due to poor percolation pathways, could contribute to the observed MI transition concomitant with ferromagnetic ordering at less than five monolayers. The disorder at the surface has also recently been compared to that at the interface with the substrate (in this case $SrTiO_3$) with *in situ* PES techniques, and it was found that the sharp t_{2g} peak at the Fermi level is greatly suppressed at the surface, while it persists at the interface.[67] The decrease in itineracy due to the suppressed DOS at the Fermi level was also verified with surface and interface conductivity experiments. Since our calculations do not include any disordered surface configurations or nonstoichiometry, future first-principles calculations could clarify these competing interactions. We have, however, shown that neither strong correlations nor octahedral distortions nor their combination are sufficient to reproduce the experimentally observed ultrathin film metal-insulator transition.

V. CONCLUSIONS

We have examined the effects of structural distortions and correlation effects on the electronic and magnetic properties of $SrRuO_3$ with first-principles calculations. We find that by including weak strong correlations with an effective Hubbard U of 0.6 eV or correction of the self-interaction error gives good agreement for bulk orthorhombic $SrRuO_3$ with the experimental spectroscopic data. The addition of the octahedral distortions leads to a narrowing of the majority spin Ru t_{2g} and O 2*p* states; however, the exchange splitting is small with respect to these bandwidths and consequently a fully insulating ground state is not obtained. A half-metallic ground state was shown to be stable by including moderate electron-electron correlation effects $U>2$ eV, which we note has not been observed experimentally.

The behavior of thin films was also examined in both cubic and orthorhombic unsupported films within the conventional LSDA approach and with weak correlations included. In neither case was the experimentally observed metal-insulator transition obtained. Since the electronic structures of surfaces are very sensitive to atomic reconstructions, we suggest that the experimentally observed metal-insulator transition could be either a consequence of extrinsic defects, an atomically disordered surface configuration, or due to dynamic spin correlation effects that are not treated in our static calculations.

ACKNOWLEDGMENTS

We thank A. Fujimori for helpful discussions and bringing our attention to correlation characteristics in the spectroscopic data. The authors also thank A. Zayak, J. Neaton, and W. Siemon for useful discussions and J. Okamoto and H. Kumigashira for providing us permission and use of the experimental PES data. This work was supported by the NSF under the grant NIRT (No. 0609377) (N.A.S.), by the SFI under Grant No. 07/IN.1/I945 (N.M.C. and S.S.) and by Seagate. J.M.R. acknowledges support from NDSEG sponsored by the DoD. Portions of this work made use of MRL Central Facilities supported by the MRSEC Program of the National Science Foundation under Award No. DMR05-20415 and the CNSI Computer Facilities at UC Santa Barbara under NSF Award No. CHE-0321368. Additional computational resources have been provided by the HEA IITAC project managed by the Trinity Center for High Performance Computing and by ICHEC.

*Corresponding author; nicola@mrl.ucsb.edu

[1] F. L. Marrec, A. Demuer, D. Jaccard, J.-M. Triscone, M. K. Lee, and C. B. Eom, Appl. Phys. Lett. **80**, 2338 (2002).
[2] K. S. Takahashi, A. Sawa, Y. Ishii, H. Akoh, M. Kawasaki, and Y. Tokura, Phys. Rev. B **67**, 094413 (2003).
[3] W. J. Gallagher and S. S. P. Parkin, IBM J. Res. Dev. **50**, 5 (2006).
[4] H. N. Lee, H. M. Christen, M. F. Chisholm, C. M. Rouleau, and D. H. Lowndes, Appl. Phys. Lett. **84**, 4107 (2004).
[5] C. H. Ahn, R. H. Hammond, T. H. Geballe, M. R. Beasley, J.-M. Triscone, M. Decroux, O. Fischer, L. Antognazza, and K. Char, Appl. Phys. Lett. **70**, 206 (1997).
[6] K. S. Takahashi, M. Gabay, D. Jaccard, K. Shibuya, T. Ohnishi, M. Lippmaa, and J.-M. Triscone, Nature (London) **441**, 195 (2006).
[7] I. Zutić, J. Fabian, and S. D. Sarma, Rev. Mod. Phys. **76**, 323 (2005).
[8] D. Awschalom and M. Flatte, Nat. Phys. **3**, 153 (2007).
[9] N. A. Spaldin and M. Fiebig, Science **309**, 391 (2005).
[10] R. Ramesh and N. A. Spaldin, Nature Mater. **6**, 21 (2007).
[11] A. Ohtomo, D. A. Muller, J. L. Grazul, and H. Y. Hwang, Nature (London) **419**, 378 (2002).

[12] A. Ohtomo and H. Y. Hwang, Nature (London) **427**, 423 (2004).
[13] H. Y. Hwang, Science **313**, 1895 (2006).
[14] M. Huijben, G. Rijnders, D. H. A. Blank, S. Bals, S. V. Aert, J. Verbeeck, G. V. Tendeloo, A. Brinkman, and H. Hilgenkamp, Nature Mater. **5**, 556 (2006).
[15] H. Yamada, Y. Ogawa, Y. Ishii, H. Sato, M. Kawasaki, H. Akoh, and Y. Tokura, Science **305**, 646 (2004).
[16] J. M. De Teresa, A. Barthélémy, A. Fert, J. P. Contour, F. Montaigne, and P. Seneor, Science **286**, 507 (1999).
[17] A. Brinkman, M. Huijben, M. van Zalk, J. Huijben, U. Zeitler, J. C. Maan, W. G. van der Wiel, G. Rijnders, D. H. A. Blank, and H. Hilgenkamp, Nature Mater. **6**, 493 (2007).
[18] D. Toyota *et al.*, Appl. Phys. Lett. **87**, 162508 (2005).
[19] H.-D. Kim, H.-J. Noh, K. H. Kim, and S.-J. Oh, Phys. Rev. Lett. **93**, 126404 (2004).
[20] J. Park, S.-J. Oh, J.-H. Park, D. M. Kim, and C.-B. Eom, Phys. Rev. B **69**, 085108 (2004).
[21] W. Siemons, G. Koster, A. Vailionis, H. Yamamoto, D. H. A. Blank, and M. R. Beasley, Phys. Rev. B **76**, 075126 (2007).
[22] P. B. Allen, H. Berger, O. Chauvet, L. Forro, T. Jarlborg, A. Junod, B. Revaz, and G. Santi, Phys. Rev. B **53**, 4393 (1996).
[23] P. Kostic, Y. Okada, N. C. Collins, Z. Schlesinger, J. W. Reiner, L. Klein, A. Kapitulnik, T. H. Geballe, and M. R. Beasley, Phys. Rev. Lett. **81**, 2498 (1998).
[24] G. Cao, S. McCall, M. Shepard, J. E. Crow, and R. P. Guertin, Phys. Rev. B **56**, 321 (1997).
[25] K. Maiti, Phys. Rev. B **73**, 235110 (2006).
[26] K. Maiti and R. S. Singh, Phys. Rev. B **71**, 161102(R) (2005).
[27] H.-T. Jeng, S.-H. Lin, and C.-S. Hsue, Phys. Rev. Lett. **97**, 067002 (2006).
[28] A. T. Zayak, X. Huang, J. B. Neaton, and K. M. Rabe, Phys. Rev. B **74**, 094104 (2006).
[29] V. M. Goldschmidt, Naturwiss. **14**, 477 (1926).
[30] N. Fukunaga and N. Tsuda, J. Phys. Soc. Jpn. **63**, 3798 (1994).
[31] A. Kanbayasi, J. Phys. Soc. Jpn. **41**, 1876 (1976).
[32] D. J. Singh, J. Appl. Phys. **79**, 4818 (1996).
[33] I. I. Mazin and D. J. Singh, Phys. Rev. B **56**, 2556 (1997).
[34] G. Santi and T. Jarlborg, J. Phys.: Condens. Matter **9**, 9563 (1997).
[35] W. Kohn and L. J. Sham, Phys. Rev. **140**, A1133 (1965).
[36] J. M. Soler, E. Artacho, J. D. Gale, A. García, J. Junquera, P. Ordejón, and D. Sánchez-Portal, J. Phys.: Condens. Matter **14**, 2745 (2002).
[37] D. Sánchez-Portal, P. Ordejón, E. Artacho, and J. M. Soler, Int. J. Quantum Chem. **65**, 453 (1997).
[38] P. Ordejón, E. Artacho, and J. M. Soler, Phys. Rev. B **53**, R10441 (1996).
[39] G. Kresse and J. Furthmüller, Phys. Rev. B **54**, 11169 (1996).
[40] G. Kresse and D. Joubert, Phys. Rev. B **59**, 1758 (1999).
[41] J. P. Perdew and A. Zunger, Phys. Rev. B **23**, 5048 (1981).
[42] D. M. Ceperley and B. J. Alder, Phys. Rev. Lett. **45**, 566 (1980).
[43] P. E. Blöchl, Phys. Rev. B **50**, 17953 (1994).
[44] We used 10 valence electrons for Sr ($4s^2 4p^6 5s^2$), 14 for Ru ($4p^6 4d^7 5s^1$), and 6 for each oxygen ($2s^2 2p^4$).
[45] H. J. Monkhorst and J. D. Pack, Phys. Rev. B **13**, 5188 (1976).
[46] P. E. Blöchl, O. Jepsen, and O. K. Andersen, Phys. Rev. B **49**, 16223 (1994).
[47] L. Kleinman and D. M. Bylander, Phys. Rev. Lett. **48**, 1425 (1982).
[48] N. Troullier and J. L. Martins, Phys. Rev. B **43**, 1993 (1991).
[49] The electronic configurations for each atom is Sr $4s^2 4p^6 4d^0 4f^0$ (1.50, 1.50, 2.00, 2.00), Ru $4s^2 4p^6 4d^7 4f^0$ (1.30, 1.30, 1.40, 1.30), and O $2s^2 2p^4 3d^0 4f^0$ (1.15, 1.15, 1.15, 1.50), where the cutoff radii for each orbital is given in parentheses.
[50] The grid cutoff mentioned is not directly comparable to the plane-wave cutoff value used to represent the wave functions in a standard plane-wave implementation of DFT; it is rather used here to represent the density, and is typically four times larger than the wave function cutoff.
[51] B. C. Chakoumakos, S. E. Nagler, S. T. Misture, and H. M. Christen, Physica B (Amsterdam) **241-243**, 358 (1997).
[52] V. I. Anisimov, F. Aryasetiawan, and A. I. Liechtenstein, J. Phys.: Condens. Matter **9**, 767 (1997).
[53] S. L. Dudarev, G. A. Botton, S. Y. Savrasov, C. J. Humphreys, and A. P. Sutton, Phys. Rev. B **57**, 1505 (1998).
[54] A. G. Petukhov, I. I. Mazin, L. Chioncel, and A. I. Lichtenstein, Phys. Rev. B **67**, 153106 (2003).
[55] A. Filippetti and N. A. Spaldin, Phys. Rev. B **67**, 125109 (2003).
[56] D. Vogel, P. Krüger, and J. Pollmann, Phys. Rev. B **54**, 5495 (1996).
[57] C. D. Pemmaraju, T. Archer, D. Sánchez-Portal, and S. Sanvito, Phys. Rev. B **75**, 045101 (2007).
[58] M. Stengel and N. A. Spaldin, Phys. Rev. B **77**, 155106 (2008).
[59] C. W. Jones, P. D. Battle, P. Lightfoot, and W. T. A. Harrison, Acta Crystallogr., Sect. C: Cryst. Struct. Commun. **45**, 365 (1989).
[60] Although in this symmetry the RuO_6 cages are rotated, we retain the standard spherical harmonics for the $4d$ orbitals described in terms of an octahedral crystal field for a cubic perovskite. The transformation from the cubic to orthorhombic d orbital reference frame requires a rotation of $\pi/4$ about the [001] direction; additionally, the octahedral units retain almost all of their integrity; i.e., the apical and axial Ru-O bond lengths are identical within 0.01 Å.
[61] L. Klein, J. S. Dodge, C. H. Ahn, J. W. Reiner, L. Mieville, T. H. Geballe, M. R. Beasley, and A. Kapitulnik, J. Phys.: Condens. Matter **8**, 10111 (1996).
[62] J. Okamoto, T. Mizokawa, A. Fujimori, I. Hase, M. Nohara, H. Takagi, Y. Takeda, and M. Takano, Phys. Rev. B **60**, 2281 (1999).
[63] K. Fujioka, J. Okamoto, T. Mizokawa, A. Fujimori, I. Hase, M. Abbate, H. J. Lin, C. T. Chen, Y. Takeda, and M. Takano, Phys. Rev. B **56**, 6380 (1997).
[64] J. Okamoto (unpublished); The material preparation and characterization follows that outlined in J. Okamoto, T. Mizokawa, A. Fujimori, I. Hase, M. Nohara, H. Takagi, Y. Takeda, and M. Takano, Phys. Rev. B **60**, 2281 (1999).
[65] Reused with permission from D. Toyota, Appl. Phys. Lett. **87** 162508 (2005). Copyright 2005, American Institute of Physics.
[66] J. Kim, J. Chung, and S.-J. Oh, Phys. Rev. B **71**, 121406(R) (2005).
[67] H. Kumigashira, M. Minohara, M. Takizawa, A. Fujimori, D. Toyota, I. Ohkubo, M. Oshima, M. Lippmaa, and M. Kawasaki, Appl. Phys. Lett. **92**, 122105 (2008).
[68] G. Herranz, N. Dix, F. Sánchez, B. Martínez, J. Fontcuberta, M. V. García-Cuenca, C. Ferrater, M. Varela, D. Hrabovsky, and A. R. Fert, J. Appl. Phys. **97**, 10M321 (2005).
[69] D. C. Worledge and T. H. Geballe, Phys. Rev. Lett. **85**, 5182 (2000).
[70] I. I. Mazin, Phys. Rev. Lett. **83**, 1427 (1999).

[71] J. M. D. Coey and S. Sanvito, J. Phys. D **37**, 988 (2004).
[72] A. F. Andreev, Sov. Phys. JETP **19**, 1228 (1964).
[73] J. Soulen, Jr. *et al.*, Science **282**, 85 (1998).
[74] S. K. Upadhyay, A. Palanisami, R. N. Louie, and R. A. Buhrman, Phys. Rev. Lett. **81**, 3247 (1998).
[75] P. Raychaudhuri, A. P. Mackenzie, J. W. Reiner, and M. R. Beasley, Phys. Rev. B **67**, 020411(R) (2003).
[76] B. Nadgorny, M. S. Osofsky, D. J. Singh, G. T. Woods, J. R. J. Soulen, M. K. Lee, S. D. Bu, and C. B. Eom, Appl. Phys. Lett. **82**, 427 (2003).
[77] J. Sanders, G. T. Woods, P. Poddar, H. Srikanth, B. D. Ski, and S. Kolesnik, Proceedings of the 49th Annual Conference on Magnetism and Magnetic Materials Vol. 97, 2005 (unpublished), p. 10C912.
[78] A. R. Rocha, V. M. Garcia-Suarez, S. Bailey, C. Lambert, J. Ferrer, and S. Sanvito, Phys. Rev. B **73**, 085414 (2006).
[79] The Brillouin zone was sampled in these cases with a $20\times20\times1$ Monkhorst-Pack mesh for the orthorhombic structure and a $40\times40\times1$ mesh for the cubic structure.
[80] F. Taddei, S. Sanvito, and C. Lambert, J. Low Temp. Phys. **124**, 305 (2001).
[81] G. Rijnders, D. H. A. Blank, J. Choi, and C.-B. Eom, Appl. Phys. Lett. **84**, 505 (2004).
[82] D. Toyota, I. Ohkubo, H. Kumigashira, M. Oshima, T. Ohnishi, M. Lippmaa, M. Kawasaki, and H. Koinuma, J. Appl. Phys. **99**, 08N505 (2006).
[83] Q. Gan, R. A. Rao, C. B. Eom, J. L. Garrett, and M. Lee, Appl. Phys. Lett. **72**, 978 (1998).
[84] Complete structural relaxation of the three-unit-cell slab within the orthorhombic symmetry did not produce significant changes in the electronic or magnetic structure.